Hearing loss mutations alter the functional properties of human P2X2 receptor channels through distinct mechanisms

Benjamin George[a], Kenton J. Swartz[a,1], and Mufeng Li[a,1]

[a]Molecular Physiology and Biophysics Section, Porter Neuroscience Research Center, National Institute of Neurological Disorders and Stroke, National Institutes of Health, Bethesda, MD 20892-3701

Edited by Richard W. Aldrich, The University of Texas at Austin, Austin, TX, and approved September 27, 2019 (received for review July 15, 2019)

Activation of P2X2 receptor channels by extracellular ATP is thought to play important roles in cochlear adaptation to elevated sound levels and protection from overstimulation. Each subunit of a trimeric P2X2 receptor is composed of intracellular N and C termini, a large extracellular domain containing the ATP binding site and 2 transmembrane helices (TM1 and TM2) that form a cation permeable pore. Whole-exome sequencing and linkage analysis have identified 3 hP2X2 receptor mutations (V60L, D273Y, and G353R) that cause dominantly inherited progressive sensorineural hearing loss (DFNA41). Available structures of related P2X receptors suggest that these 3 mutations localize to TM1 (V60L), TM2 (G353R), or the β-sheet linking the TMs to the extracellular ATP binding sites (D273Y). Previous studies have concluded that the V60L and G353R mutants are nonfunctional, whereas the D273Y mutant has yet to be studied. Here, we demonstrate that both V60L and G353R mutations do form functional channels, whereas the D273Y mutation prevents the expression of functional channels on the cell membrane. Our results show that the V60L mutant forms constitutively active channels that are insensitive to ATP or the antagonist suramin, suggesting uncoupling of the pore and the ligand binding domains. In contrast, the G353R mutant can be activated by ATP but exhibits alterations in sensitivity to ATP, inward rectification, and ion selectivity. Collectively, our results demonstrate that the loss of functional P2X2 receptors or distinct alterations of its functional properties lead to noise-induced hearing loss, highlighting the importance of these channels in preserving hearing.

purinergic | ATP | deafness | cochlea

P2X receptors are ligand-gated cation permeable channels that are activated by extracellular ATP and mediate a variety of cellular responses, including nociception, adaptive immune system responses, smooth and cardiac muscle contraction, and adaptation to loud sounds in the cochlea (1–4). P2X receptor channels assemble as homotrimeric or heterotrimeric complexes of 7 different subunits (P2X1–7) (5, 6). Each of the 7 subunits is composed of an intracellular amino terminus and carboxyl terminus, a large extracellular domain forming the ATP binding sites, and 2 α-helical transmembrane segments (TM1 and TM2) that together form the ion permeation pathway.

The P2X2 receptor is expressed in the cochlea where it is thought to localize to hair cells, as well as Reisner's membrane epithelial cells that maintain the integrity of the endolymphatic compartment (3, 7–18). ATP released into the endolymphatic compartment in response to loud noise has been proposed to activate P2X2 receptors in the Reisner's membrane and to thereby produce a cation shunt that reduces the endolymphatic potential and the driving force for sound transduction (11). P2X2-knockout mice fail to adapt to loud noise and are susceptible to overstimulation of hair cells, resulting in reduced noise-induced temporary threshold shifts and progressive noise-induced hearing loss (3, 16). Noise exposure causes up-regulation of P2X2 receptors in the organ of Corti and spiral ganglion neurons (19), further implicating their involvement in noise-induced otoprotection and suggesting the existence of an ATP-mediated adaptation mechanism to loud noise (19, 20).

Previous studies have identified 3 missense mutations (c.178G>T or p.V60L, c.601G>A or p.D273Y, and c.1057G.C or p.G353R) in the human P2X2 (hP2X2) receptor gene as the cause of autosomal dominant progressive sensorineural hearing loss (DFNA41) in 2 nonrelated Chinese families, 1 Italian family, and 1 Japanese family (16, 21–23). The disease phenotype of an autosomal dominant mutation is caused by a loss- or a gain-of-function mutation in one allele, despite the presence of a normal copy of the gene. These mutations localize to distinct regions of the protein, raising questions about how they alter protein function to cause a similar pathology. Although structures of the P2X2 receptor subtype have not yet been reported, X-ray structures have been solved for several related subtypes, including zfP2X4, AmP2X, hP2X3, and pdP2X7 (6, 24–27). These structures predict that the V60L mutation is within the external end of the TM1 helix near TM2, the D273Y mutation resides within a β-sheet structure connecting the extracellular and TM domains, and the G353R mutation is located in the middle of the pore-lining TM2 helix (Fig. 1*A*). The V60L mutation in hP2X2 receptors has been reported to result in nonfunctional channels in 2 studies (16, 28), suggesting that disease results from a loss of functional channels. However, another study examining interactions between the external ends of TM1 and TM2 in rat P2X2 (rP2X2) reported that the equivalent V48L mutation resulted in increased currents at negative holding potentials (29), suggesting that the mutant in rP2X2 may retain

Significance

In the cochlea, extracellular ATP-activated P2X2 receptor channels play important roles in adaptation to elevated sound, and several hP2X2 mutations cause inherited progressive sensorineural hearing loss. We investigated the functional properties of 3 mutants (V60L, D273Y, and G353R) and show that only the D273Y mutant results in nonfunctional channels. The V60L mutant exhibits constitutive activation and uncoupling between ATP binding and pore opening, while the G353R mutant exhibits altered sensitivity to ATP, inward rectification, and ion selectivity. Our results demonstrate that mutations in P2X2 receptors can cause hearing loss without completely disrupting channel function, highlighting the importance of these channels for protecting hearing.

Author contributions: B.G., K.J.S., and M.L. designed research; B.G. and M.L. performed research; B.G. and M.L. analyzed data; and B.G., K.J.S., and M.L. wrote the paper.

The authors declare no competing interest.

This article is a PNAS Direct Submission.

[1]To whom correspondence may be addressed. Email: kenton.swartz@nih.gov or limuf@ninds.nih.gov.

This article contains supporting information online at www.pnas.org/lookup/suppl/doi:10.1073/pnas.1912156116/-/DCSupplemental.

First published October 21, 2019.

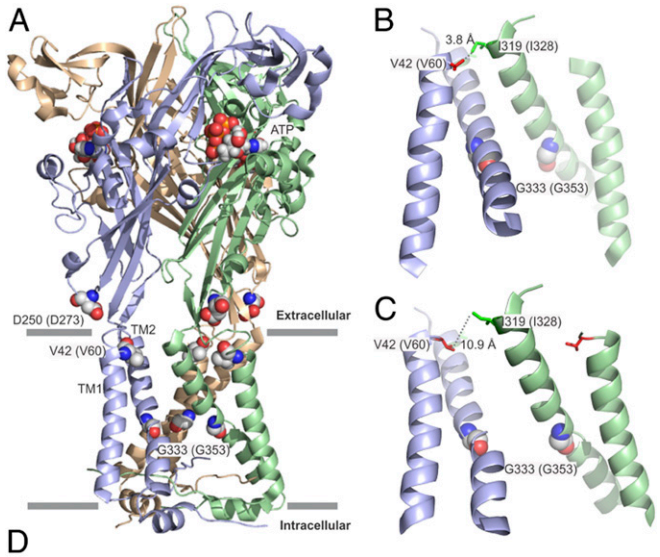

D

hP2X2	55	YFVWYVFIVQK	270	CDLDLPASEC	345	LATALTSVGVGSFLCD
rP2X2	43	YFVWYVFIVQK	258	CDLDLSESEC	334	LATALTSIGVGSFLCD
hP2X1	43	YVIGWVFLYEK	261	CDLDWHVRHC	335	IGSGIGIFGVATVLCD
hP2X3	37	YFVGWVFLHEK	247	CDLDKAWDQC	325	SVAAFTSVGVGTVLCD
hP2X4	42	YVIGWVFVWEK	261	CNLDRAASLC	339	IGSGLALLGMATVLCD
hP2X5	42	YLVVWVFLIKK	263	CDLDKAASEC	329	----------AFFCD
hP2X6	43	YVVGWALLAKK	262	CDLDTGDSGC	331	LGTGAAWLGVVTFFCD
hP2X7	40	YVC-FALVSDK	260	CNLDRWFHHC	337	IGSTLSYFGLAAVFID

Fig. 1. Location of sensorineural hearing loss mutations in P2X receptors. (*A*) Trimeric human P2X3 X-ray structure in the ATP-bound open state (PDB ID code 5svk) with each monomer in a different color (blue, green, and gold). The residues whose mutation causes hearing loss (D250, V42, and G333 in hP2X3; or D273, V60, and G353 in hP2X2) and the ATP molecules are indicated and shown as colored spheres. (*B* and *C*) Expanded view of the TM region in hP2X3 highlighting the transition in TM2 from an α-helix in the apo closed state (*B*; PDB ID code 5svj) to a 3_{10}-helix in the ATP-bound open state (*C*; PDB ID code 5svk). (*D*) Sequence alignment showing conservation of mutated residues between hP2X2 and rP2X2, and different hP2X subtypes.

some function and raising the possibility that the phenotype of the V60L mutant in hP2X2 may have been incorrectly assessed. In the case of the G353R mutation, while one study reported that the channel is nonfunctional (28), another study on rP2X2 reported responses to extracellular ATP when the equivalent Gly is mutated to Lys (30), leading us to question whether G353R in hP2X2 is indeed nonfunctional. To our knowledge, the D273Y mutation in the hP2X2 has not been previously studied. To provide a foundation for understanding how mutations in P2X2 receptors cause hearing loss and for exploring the role of P2X2 receptors in hearing protection, we reexamined how these hearing loss mutations alter the biophysical properties of the receptor.

Results

We began by characterizing the functional properties of wild-type (WT) hP2X2 receptor channels using whole-cell patch-clamp recording techniques after expressing the protein in HEK293 cells. At a holding voltage of −60 mV in the presence of a physiological extracellular solution, 2-s applications of ATP-containing extracellular solutions elicited rapid activation of a slowly desensitizing, inward current that quickly deactivated upon removal of ATP. When applied at concentrations ranging from 1 to 300 μM, we obtained a concentration–response relation for ATP activation of hP2X2 receptors with an EC_{50} of 17 ± 2 μM and a Hill coefficient (n_H) of 1.4 ± 0.2 (Fig. 2*A*). We also obtained current–voltage (*I–V*) relations by stepping the membrane voltage from −160 to +160 mV in the presence of a saturating concentration of ATP and observed large inward currents at negative membrane voltages and small outward currents at positive voltages (Fig. 2*B*), confirming the characteristic inward rectification of P2X2 receptor channels. In the absence of ATP, we observed only small inward and outward currents for cells expressing hP2X2 receptor channels (Fig. 2*B*), and these were similar to those seen in untransfected cells (Fig. 2*C*). We conclude that both the apparent affinity of hP2X2 receptors for ATP and the inward rectification of *I–V* relationships are similar to those previously reported for hP2X2 and rP2X2 receptor channels (31–34).

The G353R Mutation Alters the Gating Properties of hP2X2 Receptor Channels. The G353R mutation in TM2 was identified in an Italian family affected by autosomal dominant nonsyndromic hearing loss (21). Although structures of P2X2 receptors have not yet been reported, X-ray structures of the homolog hP2X3 receptor show that opening of the pore is accompanied by a transition in the TM2 helix from an α-helix to a 3_{10}-helix within the conserved sequence G333–V334–G335 (24) (Fig. 1 *B* and *C*). hP2X3 and hP2X2 receptors are closely related (39% sequence identity), and the TM2 helix of hP2X2 receptors has an identical sequence of G353–V354–G355 in this internal region of TM2 (Fig. 1*D*). We anticipated that introduction of the G353R mutation into this region might cause dramatic alterations in the functional properties of hP2X2 receptor channels because it would position a basic residue near or within the cation permeation pathway and might also energetically perturb the α- to 3_{10}-helix transition observed during opening of hP2X3 receptor channels. Surprisingly, the G353R mutation results in channels that appear closed in the absence of ATP and that can be robustly activated by external application of ATP (Fig. 2*D*). Examination of the concentration–response relation for ATP activation of hP2X2 G353R revealed that the mutation produces a modest 2.6-fold shift of the relation to higher ATP concentrations, with an EC_{50} of 45 ± 14 μM and n_H of 1.1 ± 0.2 (Fig. 2*A*).

Examination of *I–V* relations for the hP2X2 G353R mutant also shows that the strong inward rectification seen in the WT receptor channel is preserved in the mutant (Fig. 2 *B* and *D*). Closer inspection of those relationships for the WT and mutant receptor, however, reveal that the mutation increases the steepness of the *I–V* relationship at negative membrane voltages (Fig. 2 *B* and *D*). Although the molecular mechanism of inward rectification in P2X2 receptor channels is not fully understood, it does not seem to occur by the type of pore-blocking mechanism seen in inwardly rectifying K^+ channels (35–39) and is thought to result from a voltage-dependent gating transition and change in single-channel conductance (32, 33). To investigate these alterations in inward rectification further, we obtained macroscopic conductance–voltage (*G–V*) relationships for hP2X2 WT and the G353R mutant by measuring tail current amplitudes elicited by stepping membrane voltage to −60 mV following each test pulse (Fig. 2 *E* and *F*). Although saturation of tail current amplitudes could not be reliably determined at voltages as negative as −200 mV for either the WT or mutant receptor, inspection of the overall *G–V* relationships reveals that the mutation produces a shift of the relationship to more negative membrane voltages (Fig. 2*F*). Fitting of a Boltzmann equation to both *G–V* relationships shows that the G353R mutation shifts the midpoint ($V_{1/2}$) by about −60 mV (from −122 mV for WT to −184 mV for G353R) and increases the valence from 0.5 to 0.6 (Fig. 2*F*). Although activation of the G353R mutant by extracellular ATP is largely preserved, this mutation clearly alters the mechanism of inward rectification.

Given that the G353R mutation introduces a basic residue into or near the ion permeation pathway (Fig. 1*A*), we investigated whether the mutation altered the ion selectivity of P2X2 receptors. The P2X2 receptor channel is a relatively nonselective cation channel that has a measurable permeability to the large organic cation *N*-methyl-D-glucamine ($NMDG^+$) and is Ca^{2+} permeable

PHYSIOLOGY

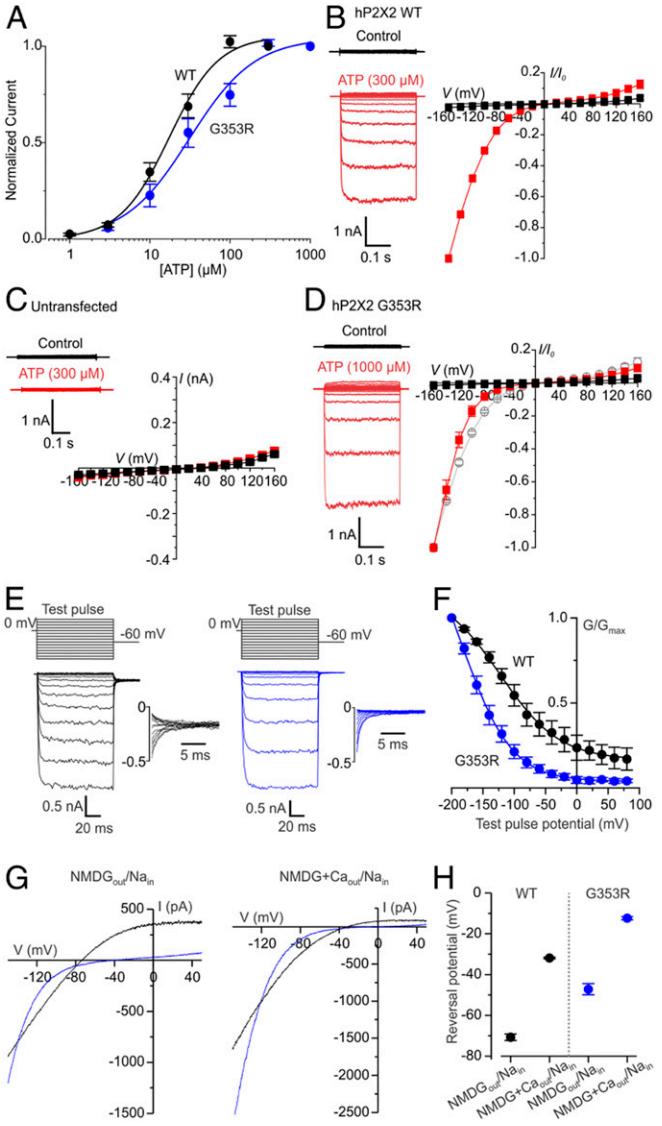

Fig. 2. Functional properties of hP2X2 WT and G353R mutant channels. (*A*) Normalized concentration–response relations for ATP activation for hP2X2 WT (black circles; $n = 6$) and the G353R mutant (blue circles; $n = 5$). Current amplitude measured with test concentrations were individually normalized to the current amplitude measured at the control concentration to generate the ATP concentration–response relations. The solid lines represent fits of the Hill equation to the data resulting in an $EC_{50} = 17 \pm 2$ μM and $n_H = 1.4 \pm 0.2$ for WT and $EC_{50} = 45 \pm 14$ μM and n_H of 1.1 ± 0.2 for G353R. (*B*) Currents elicited by voltage steps (−160 to +160 mV; $V_{hold} = 0$ mV; pulses were given at 20-mV increments every 2 s) applied to cells transfected with hP2X2 WT in control solution (black) and after application of 300 μM ATP (red). Normalized plot of current–voltage relationships shown to the *Right* are for hP2X2 in control solution (black) and after application of external ATP (red). The data points are mean steady-state current ± SEM ($n = 6$), normalized to current at −160 mV in the presence of ATP. (*C*) Currents elicited by applying voltage steps (−160 to +160 mV; $V_{hold} = 0$ mV; pulses were given at 20-mV increments every 2 s) to an untransfected cell in control solution (black) and 300 μM ATP (red). Current–voltage relationships for untransfected cells ($n = 9$) in control solution (black) and 300 μM ATP (red). (*D*) Currents elicited by voltage steps (−160 to +160 mV; $V_{hold} = 0$ mV; pulses were given at 20-mV increments every 2 s) applied to cells transfected with hP2X2 G353R in control solution (black) and after application of ATP (red). Normalized plot of current–voltage relationships shown to the *Right* as in *B* with $n = 9$. The open gray circles represent data for WT taken from *B*. (*E*) Currents elicited by applying voltage steps from −200 to +80 mV in 20-mV increments from a holding potential of 0 mV. Tail currents were recorded at −60 mV, and their enlargements are shown on the *Right*. ATP-activated currents are shown after subtracting control currents recorded in the absence of ATP. The black traces (*Left*) were recorded from a cell expressing hP2X2 WT, and blue traces (*Right*) from a cell expressing the G353R mutant. (*F*) Normalized *G–V* relationships derived from the tail current measurements as in *E*. The black filled circles are hP2X2 WT ($n = 4$), and the blue filled circles are G353R ($n = 4$). The smooth curves are fits of the Boltzmann equation to the data with $V_{1/2}$ and z values of −122 mV and 0.5 for hP2X2 and −184 mV and 0.6 for G353R. (*G*) Currents elicited by voltage ramps from −150 to +50 mV (1-s duration) from a holding potential of −60 mV in either $NMDG_{out}/Na_{in}$ solutions (*Left*) or $NMDG+Ca_{out}/Na_{in}$ solutions (*Right*). Currents elicited by ramps in the absence of ATP have been subtracted from those elicited in the presence of ATP to obtain ATP-activated currents. The black current traces are hP2X2 WT, and the blue traces are G353R. (*H*) Summary of the reversal potentials measured for hP2X2 WT (black; $n = 4$) and G353R (blue; $n = 4$) in either $NMDG_{out}/Na_{in}$ solutions or $NMDG+Ca_{out}/Na_{in}$ solutions as shown in *G*.

(40–43). To test this possibility, we measured reversal potentials (V_{rev}) for WT and G353R channels in the presence of 140 mM Na^+ in the intracellular solution and either 140 mM $NMDG^+$ or 140 mM $NMDG^+$ plus 10 mM Ca^{2+} in the extracellular solution (Fig. 2 *G* and *H*). Remarkably, we measured less negative V_{rev} values for G353R in $NMDG_{out}/Na_{in}$ solutions compared to WT, demonstrating that this mutant has higher permeability to $NMDG^+$ ($P_{NMDG/Na} = 0.06$ for WT and 0.16 for G353R). When 10 mM Ca^{2+} is added to the extracellular $NMDG^+$ solution, the reversal potentials are shifted from −71 to −32 mV for hP2X2 WT, and from −32 to −12 mV for G353R, indicating that both channels are Ca^{2+} permeable and that the mutant likely also increases the relative permeability to Ca^{2+}. Taken together, these results reveal that, although the G353R mutant channel is functional, it exhibits marked alterations in inward rectification and in ion selectivity.

The D273Y Mutant Channel Does Not Traffic to the Plasma Membrane. The D273Y mutation was identified in 2 patients suffering mitochondrial encephalomyopathy, lactic acidosis, and stroke-like episodes (MELAS), as well as severe sensorineural hearing loss (22). It was proposed that P2X2 activation is suppressed in those patients stemming from mitochondrial mutations that decrease ATP production (22), but the effect of the D273Y mutation on P2X2R function was not tested. We expressed the hP2X2 D273Y mutant in HEK293 cells and looked for evidence of channel activity when applying voltage steps from −160 to +160 mV in the absence or presence of a high concentration of ATP (Fig. 3 *A* and *B*). However, we measured only small currents in either the absence or presence of ATP that were comparable to those observed in untransfected cells (Fig. 2*C*). Interestingly, this Asp is highly conserved across 7 P2X subtypes of different species (Fig. 1*D*), suggesting an important functional or structural role in all P2X receptor channels. Consistent with this inference, we also did not detect ATP-activated currents on cells expressing the equivalent mutation (D261Y) in rP2X2 (Fig. 3 *C* and *D*).

To investigate whether this mutant channel is nonfunctional or fails to traffic to the plasma membrane, we used confocal microscopy together with immunocytochemistry to examine membrane expression of the D261Y mutation in rP2X2, against which many commercial antibodies are available. We also expressed P2X2 constructs tagged in the C terminus with the Clover fluorescent protein to confirm the antibody specificity and independently verify the cellular location of the protein. To test the functionality of the tagged protein, we obtained current–voltage (*I–V*) relations for the rP2X2–WT–Clover tagged construct by stepping membrane voltage from −160 to +160 mV in the presence of a saturating concentration of ATP and observed large inward currents at negative membrane voltages and small outward currents at positive voltages, confirming the characteristic inward rectification of P2X2 receptor channels (Fig. 3 *E* and *F*). Confocal images of cells transfected with rP2X2–WT–Clover

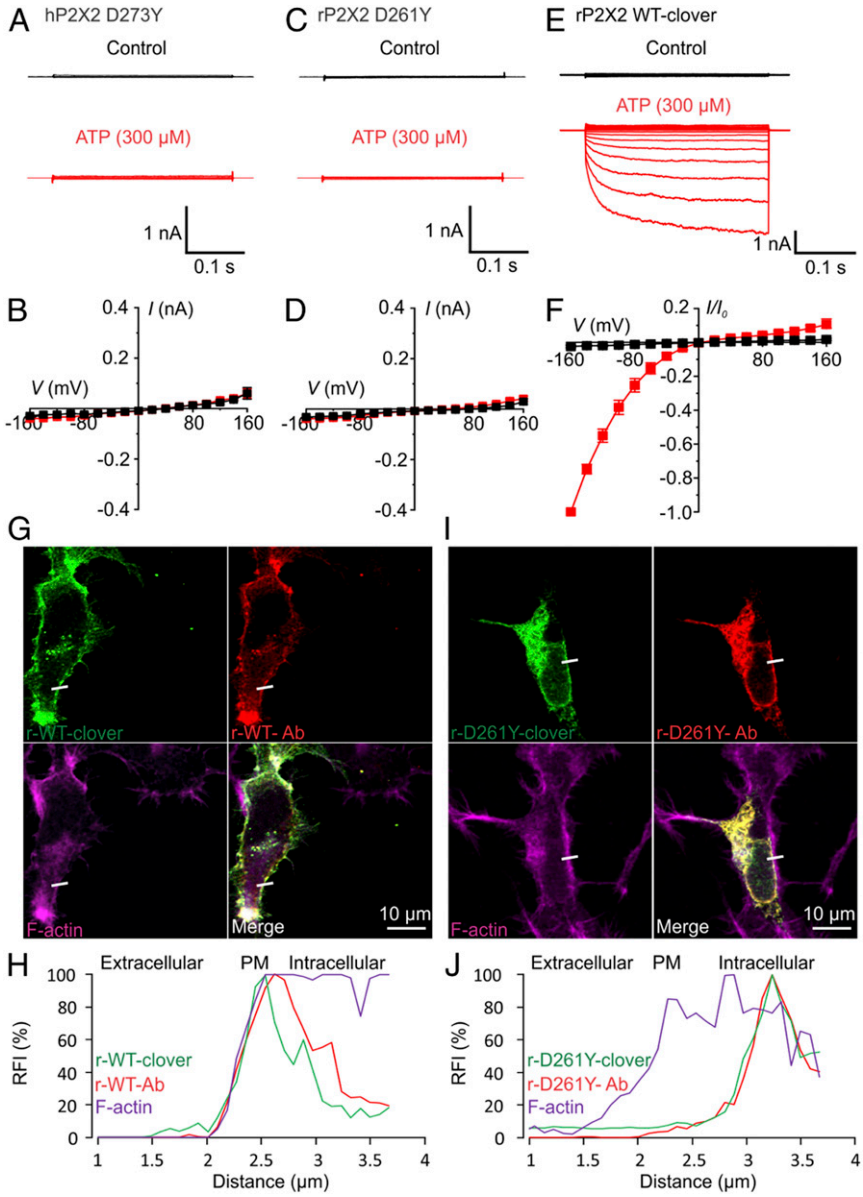

Fig. 3. D273Y channels fail to traffic to the plasma membrane. (*A*) Currents elicited by applying voltage steps (−160 to +160 mV; V_{hold} = 0 mV; pulses were given at 20-mV increments every 2 s) to a HEK cell transfected with the hP2X2 D273Y mutant in the absence (black) or presence (red) of external ATP. (*B*) Plot of current–voltage relationships obtained from cells transfected with hP2X2 D273Y in the absence (black) or presence (red) of external ATP (n = 5). (*C*) Currents elicited by applying voltage steps (−160 to +160 mV; V_{hold} = 0 mV; pulses were given at 20-mV increments every 2 s) to a HEK cell transfected with the Clover-tagged rP2X2 D261Y mutant in the absence (black) or presence (red) of external ATP. (*D*) Plot of current–voltage relationships obtained from cells transfected with the Clover-tagged rP2X2 D261Y mutant in the absence (black) or presence (red) of external ATP (n = 5). (*E*) Currents elicited by applying voltage steps (−160 to +160 mV; V_{hold} = 0 mV; pulses were given at 20-mV increments every 2 s) to a HEK cell transfected with Clover-tagged rP2X2 in the absence (black) or presence (red) of external ATP. (*F*) Plot of current–voltage relationships obtained from cells transfected with Clover-tagged rP2X2 in the absence (black) or presence (red) of external ATP (n = 5). (*G*) Representative confocal images of HEK cells expressing Clover-tagged rP2X2 (green) stained with an anti-P2X2 antibody followed by a secondary Alexa Fluor 555-conjugated goat anti-rabbit (red), and Alexa Fluor 647 phalloidin to visualize F-actin (magenta). (*H*) Normalized relative fluorescence intensity profile for Clover-tagged rP2X2, the rP2X2 antibody, and F-actin fluorescence across the cell edge from the exterior to the interior of the cell showing accumulation of the 3 fluorophores at the cell edge. (*I*) Representative confocal images of HEK cells expressing Clover-tagged rP2X2 D261Y stained as in *G*. (*J*) Relative fluorescence intensity profile for Clover-tagged rP2X2 D261Y, an anti-rP2X2 antibody, and F-actin fluorescence across the cell edge showing intracellular expression of the rP2X2 D261Y mutant. The white lines across the cell edges in *G* and *I* indicate the random regions chosen to visualize the RFI profiles.

showed little intracellular accumulation of the tagged protein and a labeling pattern that resembles the plasma membrane. Cells expressing rP2X2–Clover were labeled with the anti-P2X2 antibody highlighting the specificity of this antibody (Fig. 3*G*). Additional inspection of the fluorescence profiles across the cell edge from the exterior to the interior of the cells revealed accumulation of rP2X2 WT–Clover and anti-P2X2 antibody to the edge of the cell membrane where the actin cytoskeleton is enriched, as indicated by an intense F-actin signal (Fig. 3*H*).

In contrast, confocal images of cells expressing rP2X2–D261Y–Clover revealed that there are more channels in the interior of the cell compared to WT (Fig. 3*I*). Normalized relative fluorescence showed no overlap of anti-P2X2 or rP2X2–D261Y–Clover with F-actin at the cell edge (Fig. 3*J*), suggesting that rP2X2 D261Y

channels accumulate in the cell interior and thus do not traffic efficiently to the plasma membrane as observed with the rP2X2–WT–Clover. Although the morphology of HEK cells is not optimal for demonstrating localization of the mutant to the endoplasmic reticulum (ER), our results show that the mutant is not expressed on the plasma membrane and would be consistent with retention in the ER. These findings suggest that the D261Y mutant in rP2X2 (and by extension the D273Y mutant in hP2X2) interrupts channel trafficking, presumably because the mutant does not fold properly or cannot assume a conformation that can be inserted into the surface membrane.

The V60L Mutation Causes Constitutive Activation of hP2X2 Receptor Channels. The V60L mutation was the first identified hP2X2 receptor channel mutation associated with progressive sensorineural hearing loss and was reported to produce nonfunctional channels that cannot be activated by ATP (16, 28). However, when we expressed the hP2X2 V60L mutant channels in HEK cells, we observed evidence of constitutive channel activity (Fig. 4*A*). Inwardly rectifying *I–V* relations in the absence of ATP were observed for the V60L mutant (Fig. 4 *A* and *C*), and although the amplitudes of these currents were smaller than ATP-activated currents from cells transfected with the WT hP2X2 (Fig. 2*B*), they were considerably larger than those measured from untransfected cells (Fig. 4*B*). Consistent with previous reports, the V60L mutant was not responsive to external application of ATP (Fig. 4 *A* and *C*) (16, 28).

To directly test whether the constitutive currents observed in cells transfected with hP2X2 V60L arose from mutant channels with constitutive activity, we inserted a Cys residue into the pore-lining TM2 helix and examine whether the constitutive currents could be inhibited with thiol reactive methanethiosulfonate (MTS) reagents. We previously inserted Cys residues throughout the TM2 helix of the rP2X2 receptor channel and identified T336 as a position where MTS reagents do not react in the closed state, but rapidly react with the introduced Cys residues when channels are open, suggesting that this position lines the ion permeation pathway (34, 44). In addition, reaction of rP2X2 T336C with MTS-ET [2-(trimethylammonium)ethyl methanethiosulfonate] in the open state prevents channel closure following removal of ATP, further suggesting that this position resides within the actual gate region of the P2X2 receptor channel (34, 44), a conclusion that is supported by X-ray structures of other P2X receptor subtypes solved in the absence or presence of ATP (6, 24–27). We began by testing whether MTS-ET or the larger analog MTS-TPAE [2-(tripentylammonium)ethyl methanethiosulfonate] have any effect on the hP2X2 WT receptor and observed only subtle and reversible inhibitory effects of MTS-TPAE (Fig. 5*A*). We then inserted a Cys at T348C within the TM2 helix of the hP2X2 receptor, the position equivalent to T336 in rP2X2, and observed that both MTS-ET and MTS-TPAE rapidly and irreversibly inhibited the mutant receptor in the presence of ATP, suggesting that they modified the introduced Cys when the channel is open (Fig. 5*B*). In the case of MTS-ET, the extent of inhibition was not complete, and modification of the introduced Cys prevented closure of the channel following removal of extracellular ATP (Fig. 5*B*), consistent with previous results with MTS-ET modification of the equivalent position in rP2X2 (34, 44). We also measured modification rates for both MTS-ET and MTS-TPAE at holding voltages of −60 and −100 mV, and observed that modification rates for both reagents in hP2X2 T348C exhibited little voltage dependence (Fig. 5*C*), consistent with a shallow position of the introduced Cys residue within the membrane electric field, a conclusion further supported by X-ray structures of P2X receptors (6, 24–27).

Having characterized modification of hP2X2 T348C with MTS reagents, we introduced the T348C mutation into the V60L construct and observed that expression of the double mutant in

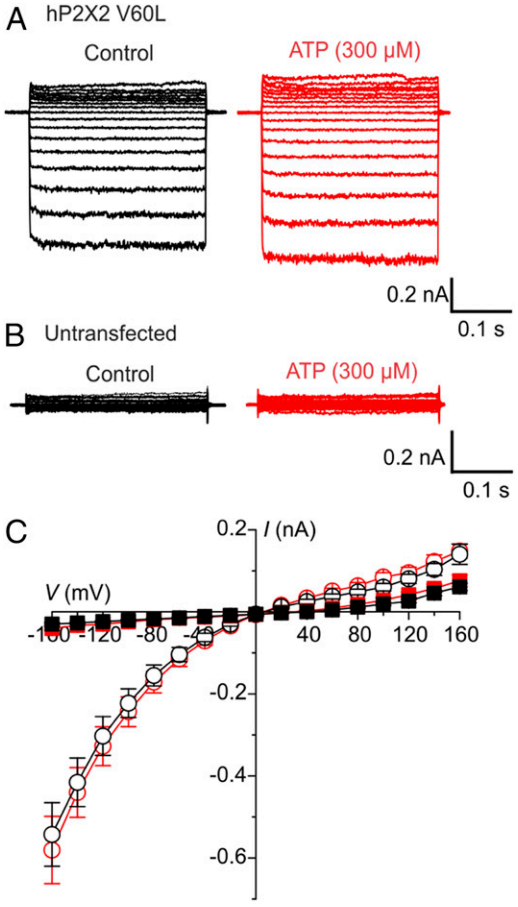

Fig. 4. Cells expressing hP2X2 V60L mutant channels exhibit constitutive inwardly rectifying currents. (*A*) Currents elicited by voltage steps (−160 to +160 mV; V_{hold} = 0 mV; pulses were executed at 20-mV increments every 2 s) to a HEK cell transfected with the hP2X2 V60L mutant in the absence (black) or presence (red) of external ATP. (*B*) Currents elicited by voltage steps (−160 to +160 mV; V_{hold} = 0 mV; pulses were executed at 20-mV increments every 2 s) to an untransfected HEK cell in the absence (black) or presence (red) of external ATP. (*C*) Plot of current–voltage relationships for cells transfected with hP2X2 V60L (open circles) (n = 5) and untransfected cells (filled squares) (n = 9) in either the absence (black) or presence (red) of external ATP (300 μM). Data points are mean ± SEM, and some error bars are smaller than symbols.

HEK cells resulted in spontaneous inwardly rectifying currents in the absence of ATP (Fig. 5*D*), consistent with what we observed with the single V60L mutation (Fig. 4 *A* and *C*). We initially examined *I–V* relations before and after application of MTS-ET to the hP2X2 T348C/V60L double mutant and observed that the MTS-ET reagent produced readily detectable inhibition of membrane currents at negative membrane voltages (Fig. 5*E*). To examine the kinetics of MTS modification of the double mutant, we held membrane voltage at 0 mV and elicited 21-s-long steps to −160 mV, a voltage where the inwardly rectifying currents are relatively large for cells expressing the V60L mutant (Fig. 6*A*). When MTS-ET was applied during the step to −160 mV, we observed only insubstantial and reversible inhibition of the hP2X2 V60L mutant (Fig. 6*A*), yet robust, rapid, and irreversible inhibition of the hP2X2 T348C/V60L double mutant (Fig. 6*A*), suggesting modification of the introduced Cys residue and directly demonstrating that the constitutive currents measured in cells expressing the V60L mutant result from ion permeation through the mutant channel. Accessibility of MTS reagents to the introduced Cys in the V60L mutant also demonstrates that

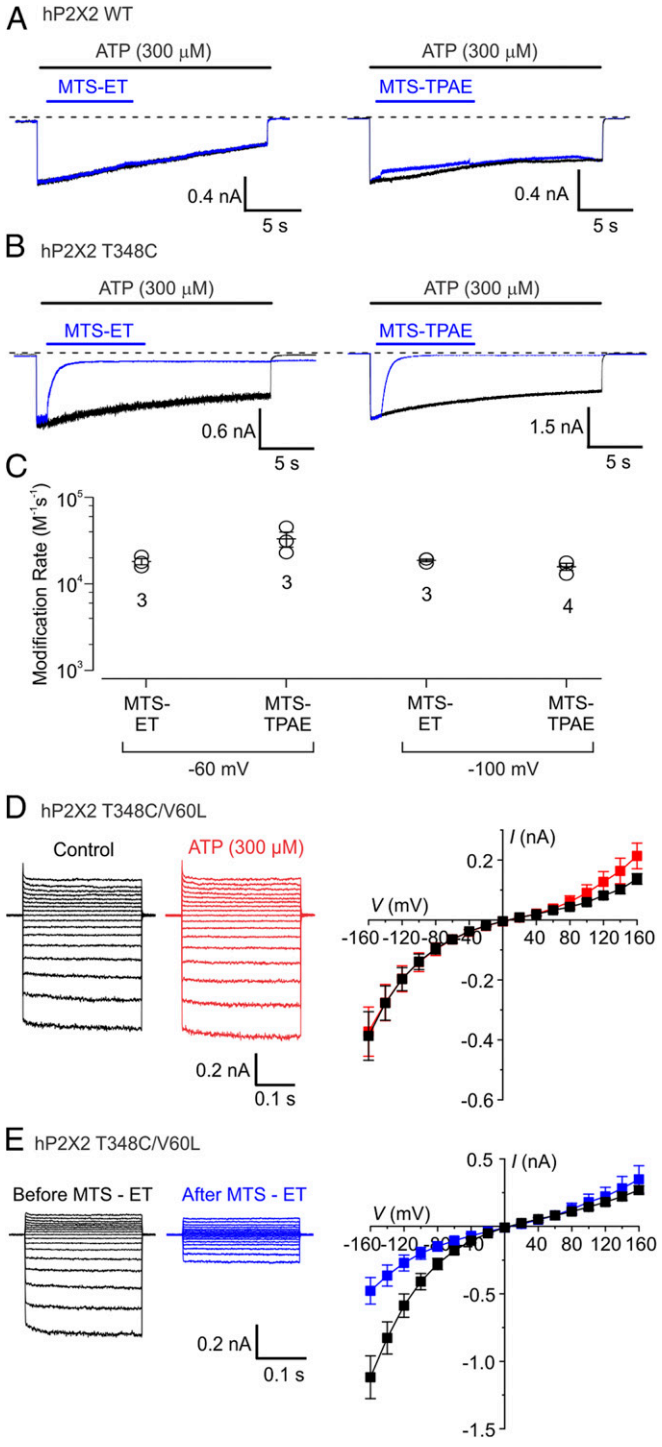

Fig. 5. Modification of hP2X2 T348C and T348C/V60L mutant channels by MTS reagents. (*A*) Superimposed currents elicited by external application of ATP to HEK cells expressing hP2X2 WT either with (blue) or without (black) subsequent external application of MTS-ET (*Left*; 100 μM) or MTS-TPAE (*Right*; 100 μM). Holding voltage is −100 mV, and the dotted lines above traces represent the zero-current level. (*B*) Superimposed currents elicited by external application of ATP to HEK cells expressing hP2X2 T348C either with (blue) or without (black) subsequent external application of MTS-ET (*Left*; 100 μM) or MTS-TPAE (*Right*; 100 μM). Holding voltage is −100 mV, and the dotted lines above traces represent the zero-current level. (*C*) Modification rates for MTS-ET and MTS-TPAE at either −60 or −100 mV for hP2X2 T348C. The symbols represent individual cells with the mean ± SEM shown using bars, with *n* values shown for each condition below the data points. (*D*) Currents elicited by voltage steps (−160 to +160 mV; V_{hold} = 0 mV; pulses were given at 20-mV increments every 2 s) to a HEK cell transfected with hP2X2 V60L/T348C in the absence (black) or presence (red) of external ATP. Plot of current–voltage relationships for hP2X2 V60L/T348C transfected cells is shown to the *Right* in the absence (black) and presence (red) of external ATP. Data points are mean ± SEM of cells (n = 5), and some error bars are smaller than symbols. (*E*) Currents elicited by voltage steps (−160 to +160 mV; V_{hold} = 0 mV; pulses were given at 20-mV increments every 2 s) to a HEK cell transfected with the hP2X2 V60L/T348C mutant before (black) and after (blue) external application of MTS-ET (100 μM). Plot of current–voltage relationships to the *Right* for V60L/T348C-transfected cells before (black) and after (blue) MTS-ET application. Data points are mean ± SEM (n = 7), and some error bars are smaller than symbols.

the pore is in an open conformation because the activation gate controls access to this Cys residue in both rP2X2 and hP2X2 receptor channels (Fig. 5) (34, 44). The rate of MTS-ET modification of the double mutant was comparable to that measured for the hP2X2 T348C mutant in the presence of a saturating concentration of ATP (Fig. 6*B*), suggesting that the double mutant has an open probability that is similar to the maximal open probability of the T348C single mutant. Interestingly, when MTS-TPAE was applied to the double mutant, we observed considerably slower modification when compared to hP2X2 T348C at a saturating concentration of ATP (Fig. 6*B*), suggesting that there is an alteration in the structure of the external pore produced by the V60L mutant.

The constitutive activation and insensitivity to ATP we observed in the V60L mutant suggest that the mutant functionally uncouples the pore from the ATP binding sites in the extracellular domain. To further explore this possibility, we examined whether the antagonist suramin might affect the constitutively active V60L channel currents. Suramin is a large polysulfonated molecule and is one of the most widely used P2X receptor antagonists (45–49). Suramin can also act as a weak agonist when a pore-lining residue in the gate region of rP2X2 is mutated (T339G) (50), suggesting that binding of suramin can induce distant conformational changes in the protein. The effect of suramin on hP2X2 has not been studied, so we first tested whether 1 mM suramin, a concentration reported to robustly inhibit rP2X2 (47–53), would affect hP2X2 receptor channel currents. Although suramin produced detectable inhibition of ATP-activated hP2X2 currents, the extent of inhibition was considerably less than that on rP2X2 (Fig. 7*A* and *SI Appendix*, Fig. S1*A*). Similar species differences in the inhibitory properties of suramin have been reported for mP2X1/hP2X1 and rP2X4/hP2X4, and it has been shown to result from amino acid differences in or near the agonist binding pocket (53, 54). When 1 mM suramin alone was applied to hP2X2- or rP2X2-expressing cells, there was no detectable agonist activity (Fig. 7*E* and *SI Appendix*, Fig. S1*C*). To further explore differences in the action of suramin on rP2X2 and hP2X2, we constructed concentration–response relations for ATP activation of hP2X2 over a range of suramin concentrations and used Schild analysis to test whether the inhibitor obeys a simple competitive mechanism and determine its affinity. The results show that the concentration–response relations are similar in shape, and they shift to higher ATP concentrations as the concentration of suramin increases (Fig. 7*B*). The slope of the Schild plot was 0.7, somewhat less than the value of 1 expected for a simple competitive mechanism, and the affinity of suramin is around 41 μM (Fig. 7*B*), considerably less than that reported for rP2X2 receptors (48, 49). Having characterized the activity of suramin on hP2X2 receptors, we tested whether suramin binding would affect the constitutive activity produced by the V60L mutant in hP2X2 or the equivalent mutation (V48L) in rP2X2. V48L in rP2X2 shows similar constitutive activation, producing inwardly rectifying *I–V* relations and insensitivity to ATP (*SI Appendix*, Fig. S1*B*). However, for the

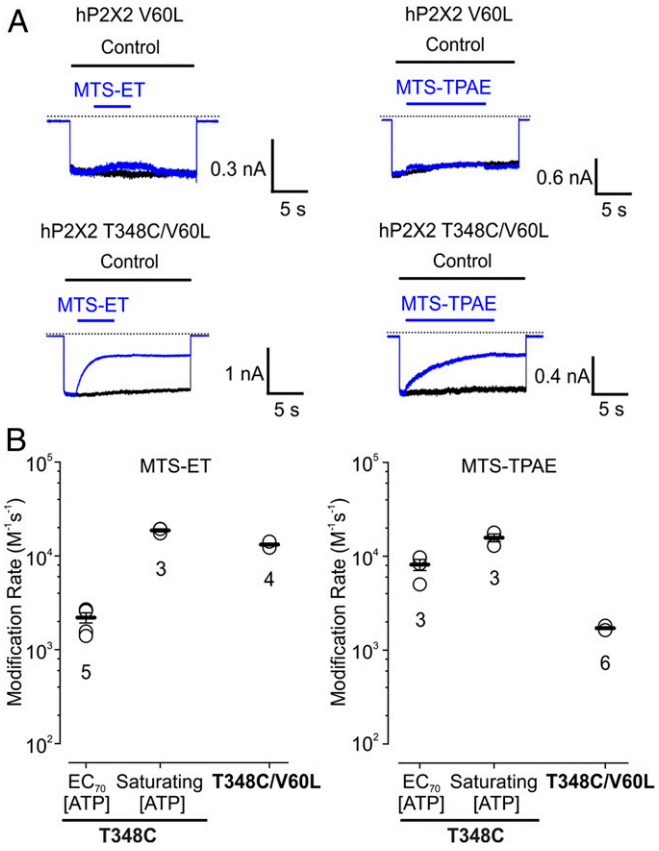

Fig. 6. Rates of MTS reagent modification of hP2X2 T348C/V60L mutant channels. (*A*) Superimposed current traces for hP2X2 V60L and V60L/T348C with 21-s-long steps from 0 to −160 mV either with (blue) or without (black) a 5-s external application of MTS-ET or an 11-s external application of MTS-TPAE. The dotted line above traces represents the zero-current level. (*B*) Rates for MTS-ET and MTS-TPAE modification of hP2X2 T348C and T348C/V60L. The symbols represent individual cells with the mean ± SEM shown using bars, with *n* values shown for each condition below the data points. Data for hP2X2 T348C were obtained at −100 mV and are from Fig. 5*C* for saturating ATP, while data for hP2X2 T348C/V60L were obtained at −160 mV. Error bars are SEM.

equivalent mutants in hP2X2 (V60L) and rP2X2 (V48L), suramin had no discernable effect on the constitutive currents (Fig. 7*D* and *SI Appendix*, Fig. S1*B*). Taken together, we conclude that the V60L mutation produces constitutive activation of hP2X2 receptors by functionally uncoupling the extracellular ligand binding and pore domains.

Discussion

Naturally occurring disease-related mutations provide unique opportunities for understanding human protein functions. Here, we studied 3 hearing loss mutations in hP2X2 receptors and found that while D273Y results in nonfunctional channels, V60L and G353R are conductive channels with diminished response to ATP, revealing the importance of full-strength activation of hP2X2 receptors in hearing protection.

One of the most abundant disease-associated mutations found in human transmembrane proteins is the Gly-to-Arg alteration, which is frequently observed in the center of the lipid bilayer (55). The G353R mutation within the TM2 of hP2X2 falls into this category and was thought to be nonfunctional (28). However, our results show that this protein forms functional ATP-activated channels on the cell surface, albeit with somewhat diminished ATP sensitivity, altered inward rectification, and ion selectivity (Fig. 2). The G353R mutant is positioned within the conserved G–V–G motif in TM2 where mutations have been shown to perturb inward rectification (30, 33, 56), consistent with this region playing an important role in the underlying mechanism. The increase in valence for the G–V relation measured for G353R likely arises from the introduction of a basic residue into a region of TM2 that resides within the membrane electric field (Fig. 1). It is also interesting that recent structures of P2X3 receptors reveal that this internal region of TM2 undergoes a transition from an α-helix to a 3_{10}-helix upon binding ATP (Fig. 1 *B* and *C*) (24), demonstrating that this region of the TM2 helix is conformationally dynamic. That the G353R mutant alters inward rectification provides motivation to further investigate this interesting and unresolved feature of gating in P2X receptor channels.

Previous studies have reported expression of P2X2 receptor channels in auditory hair cells, as well as in epithelial cells of the Reisner's membrane between the endolymphatic compartment (an extracellular solution containing high K^+, low Na^+ and Ca^{2+} in contact with the apical side of hair cell stereocilia) and the perilymphatic compartment (containing typical extracellular ion composition) (4, 8, 14, 17, 18). The alterations in ion selectivity we observe for the G353R mutation (Fig. 2 *G* and *H*) could be significant in both of these cell types. The substantial changes in inward rectification we observed for the G353R mutation would be expected to have a major impact on the ability of P2X2 receptors to produce a shunt conductance across Reisner's membrane because the voltage difference between the endolymphatic and perilymphatic compartments is only about +80 to 100 mV, a voltage difference where the conduction properties of the mutant are greatly diminished (Fig. 2*F*) (57, 58). By comparison, the voltage difference between the endolymphatic compartment and the inside of hair cells is about 125 mV, a voltage where the G353R mutant has considerable conductance. It would be interesting to explore the influence of the G353R mutant in Reisner's membrane epithelial cells and hair cells to better understand how the gating and permeation properties of the P2X2 receptor contribute to the role these channels play in protection from hearing loss.

Our results with the V60L mutation demonstrate that this channel is also functional, but in this case gives rise to constitutively active inwardly rectifying channels in the absence of ATP (Figs. 4–7), explaining why the V48L mutation in rP2X2 results in increased holding currents at negative membrane voltages (29). The inward rectification of membrane currents measured from cells expressing V60L mutant are distinguishable from small leak currents measured in untransfected cells (Fig. 4), and they are inhibited by MTS reagents following introduction of a Cys residue within the external pore (Figs. 5 and 6), demonstrating that they arise from ion permeation through an open state of the mutant channel. Our results also show that V60L mutant cannot be further activated by ATP, perhaps explaining why previous studies overlooked the constitutive activation we observed and incorrectly concluded that the protein is nonfunctional (16, 28). The insensitivity of V60L to ATP, when considered together with the observation that this mutant cannot be inhibited by the competitive antagonist suramin (Fig. 7), suggest that the mutation uncouples binding of ATP and opening of the pore to produce a constitutively open channel. Although the rate of MTS-ET modification of the introduced Cys in V60L is similar to that observed in the single Cys mutant in the presence of saturating concentrations of ATP, the rate of MTS-TPAE modification is considerably slower (Fig. 6), suggesting that the larger MTS reagent can detect a structural change in the outer pore of V60L. The V60L mutant is located at the external end of TM1 where the available structures of P2X receptors suggest that it interacts with residues projecting out from the pore-lining TM2 helix, and importantly that these interactions

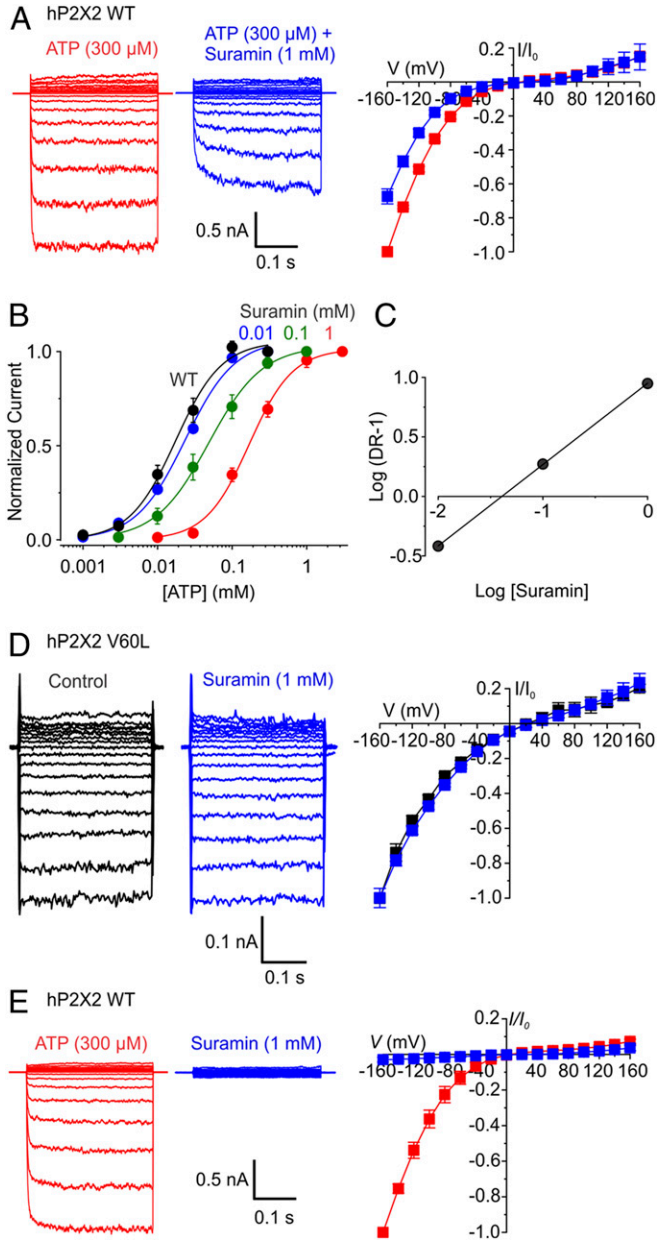

Fig. 7. Suramin does not inhibit constitutive activation of hP2X2 V60L mutant channels. (*A*) Current elicited by voltage steps (−160 to +160 mV; V_{hold} = 0 mV; pulses were given at 20-mV increments every 2 s) for hP2X2 WT in the presence of external ATP (red) or external ATP plus suramin (blue). Normalized plot of current–voltage relationships shown to the *Right*, where data points are mean steady-state currents ± SEM (n = 5), normalized to current at −160 mV in the presence of ATP alone. (*B*) Normalized concentration–response relations for ATP activation for hP2X2 WT without antagonist (filled black circles; n = 6), and in the presence of 0.01 mM suramin (filled blue circles; n = 3), 0.1 mM suramin (filled green circles; n = 3), and 1 mM suramin (filled red circles; n = 3). Current amplitude measured with test concentrations were individually normalized to the current amplitude measured at the control concentration to generate the ATP concentration–response relations. The solid lines represent fits of the data to the Hill equation resulting in an EC_{50} = 17 ± 2 μM and n_H = 1.4 ± 0.2 for control, EC_{50} = 23.5 ± 2.9 μM and n_H of 1.3 ± 0.2 for 0.01 mM suramin, 48.8 ± 3.7 μM and n_H of 1.2 ± 0.1 for 0.1 mM suramin, and 168 ± 14 μM and n_H of 1.5 ± 0.2 for 1 mM suramin. (*C*) Schild plot for suramin antagonism of hP2X2 activation with ATP. Dose ratio (DR) was calculated by dividing the EC_{50} in the presence of suramin with the EC_{50} in the absence of suramin. The slope of the Schild plot is 0.7 ± 0.003, and the K_d for suramin obtained from the x intercept was 41 ± 1 μM. (*D*) Current elicited by voltage steps (−160 to +160 mV; V_{hold} = 0 mV; pulses were given at 20-mV increments every 2 s) for hP2X2 V60L in the presence of control solution (black) or suramin (blue). Normalized plot of current–voltage relationships shown to the *Right* where data points are mean steady-state currents ± SEM (n = 3), normalized to current at −160 mV in the presence of control solution alone. (*E*) Current elicited by voltage steps (−160 to +160 mV; V_{hold} = 0 mV; pulses were given at 20-mV increments every 2 s) for hP2X2 WT in the presence of external ATP (red) or external suramin alone (blue). Normalized plot of current–voltage relationships shown to the *Right* as in *A* with n = 3. In all panels, error bars are SEM and some error bars are smaller than symbols.

would change in response to binding of ATP (Fig. 1 *B* and *C*) (24, 59). Indeed, several previous functional studies have shown that the equivalent residue in TM1 of rP2X2 (V48) interacts with I328 in TM2 to stabilize the closed state of the channel (29, 60). One reasonable interpretation is that the V60L mutation disrupts the interaction between V60 and I319 in hP2X2 to destabilize the closed state of the channel and to induce spontaneous opening.

The behavior of the V60L mutant can be described as having both gain and loss of function. The constitutively active V60L channels have a high open probability as suggested by the fast reaction rates of MTS-ET with the pore-lining Cys substitution. However, even with this high open probability, the macroscopic currents of V60L in our overexpression system are of modest amplitude, suggesting that the mutant might have a lower single-channel conductance. The slower modification rate we observed for the larger thiol-reactive compound MTS-TPAE and the pore-lining Cys would be consistent with a narrower external pore in the open state of the channel when compared to the WT hP2X2. While it is possible that the spontaneous currents contribute to the hearing loss phenotype, it seems more likely that the hearing loss phenotype is related to decoupling between ligand binding and pore opening, preventing the hP2X2 receptor from providing a substantial cation shunt when ATP is released in response to elevated sounds. It would be interesting to explore whether the constitutive conductance, an apparent gain of function with respect to ion permeability, is accompanied by other compensatory changes in the cochlea, whether it alters the ionic composition of the cochlear duct or the excitability of hair cells (3), or even leads to a down-regulation of P2X2 receptors.

In addition, we characterized the D273Y mutation, which has not been previously investigated. We find that the D273Y mutation does not form functional channels on the plasma membrane, failing to be detected on the surface membrane using confocal microscopy or to give rise to measurable currents in patch-clamp recordings (Fig. 3). The D273Y mutation was identified in a MELAS family carrying a mitochondrial 3243AG mutation and the proposed explanation for hearing loss in the family members was decreased ATP production (22). However, our results show that the hearing loss in this family likely results from loss of P2X2 channel function since the D273Y mutation indeed fails to traffic to the surface membrane and cells expressing this mutant lack P2X2 currents.

Taken together, our results reveal 3 distinct molecular mechanisms by which mutations in hP2X2 receptor channels cause autosomal-dominant progressive sensorineural hearing loss. Although the perturbations of the channel function for the V60L and G353R mutations are less severe than the D273Y mutation, it is noteworthy that the progressive hearing loss observed for all 3 are similar (16, 21, 22), suggesting that the functional properties of WT P2X2 receptors are critical for protection from hearing loss. Since the G353R mutation forms functional channels, we speculate that allosteric activators of P2X2 receptors might have therapeutic value. Developing therapeutic interventions for the V60L mutant might focus on discovering allosteric modulators

that stabilize the closed state of the channel and thereby restore functional coupling between ATP binding and pore opening.

Materials and Methods

Expression Constructs. rP2X2 in pcDNA1 was generously provided by Dr. David Julius, University of California, San Francisco, CA. hP2X2 in pCMV6 was purchased from OriGene and then subcloned into pcDNA3.1. The rP2X2 receptor in pcDNA1 and hP2X2 receptor in pcDNA3.1 were modified to single and double mutants using the QuikChange II technique (Agilent Technologies). All of the cDNAs generated for and used in this study were confirmed by DNA sequencing (Macrogen).

The equivalent mutation to D201Y described in the hP2X2 variant 6 (NM_01226.4) (22) was introduced in the hP2X2 variant 1 (Uniprot identifier Q9UBL9-1) and rP2X2 variant 1 (Uniprot identifier P49653-1), which correspond to residues D273Y and D261Y, respectively. Clover-tagged rP2X2 receptors were generated by linking Clover to rP2X2 C-terminal with a GASGAS linker.

Electrophysiology. Membrane currents were recorded from HEK293 cells using the whole-cell patch-clamp technique. Membrane voltage was controlled using an Axopatch 200B patch-clamp amplifier (Axon Instruments); currents were filtered at 2 kHz and digitized on-line using a Digidata 1440A interface board and pCLAMP 10 software with a sampling rate of 10 kHz (Axon Instruments).

For whole-cell patch-clamp recordings, HEK293 cells were seeded on a glass coverslip deposited into a 35-mm Petri dish (Corning) in Dulbecco's modified Eagle medium (DMEM) (Invitrogen) containing 10% FBS and 0.5% gentamycin and transfected with 500 to 900 ng of cDNA per well using the Fugene 6 reagent (Promega). Cells were then used for electrophysiology recordings 16 to 32 h after transfection. The standard extracellular solution contained the following: 140 mM NaCl, 5.4 mM KCl, 2 mM $CaCl_2$, 0.5 mM $MgCl_2$, 10 mM Hepes, and 10 mM D-glucose, and was adjusted to pH 7.3 with NaOH, osmolarity ~318 mmol/kg. The extracellular solution for measuring $NMDG^+$ permeability contained the following: 140 mM NMDG free salt and 10 mM Hepes, adjusted to pH 7.3 with HCl. The pipette solution contained the following: 140 mM NaCl, 10 mM EGTA, and 10 mM Hepes, and was adjusted to pH 7.0 with NaOH, osmolarity ~300 mmol/kg. Pipette resistance was typically 2 to 3 MΩ, and series resistance was less than 8 MΩ. Series resistance was not compensated. Bath and ground chambers were connected by an agar bridge containing 3 M KCl. Extracellular solutions were rapidly exchanged (~100 ms) to ATP-containing solutions with and without MTS-ET or MTS-TPAE, using a computer-controlled perfusion system (RSC-200; Bio-Logic). Stock MTS reagents (bromide salt; Toronto Research Chemicals) were freshly made in deionized H_2O at 100 mM (prepared every 4 h), stored on ice, and diluted to the desired concentrations within 2 min of their use in experiments. To expedite the screening process, we determined the range of the concentration–response relation for ATP for every mutant by applying 6 different concentrations of ATP (e.g., 1, 3, 10, 30, 100, and 300 μM).

Concentration–response relations for ATP were obtained for WT and G353R, and the data were fit to the Hill equation according to the following:

$$\frac{I}{I_{max}} = \frac{[ATP]^{n_H}}{[ATP]^{n_H} + EC_{50}^{n_H}}.$$

I is the normalized current at a given ATP concentration, I_{max} is the maximum normalized current, EC_{50} is the concentration of ATP that evokes half-maximal currents, and n_H is the Hill coefficient.

For the analyses of G–V relationships, a Boltzmann equation was fit to inward tail current vs. voltage relations using the following equation:

$$I = I_{min} + \frac{I_{max} - I_{min}}{1 + e^{\frac{zF}{RT}(V - V_{1/2})}},$$

where R is the gas constant, T is the temperature in kelvin, and F is Faraday's constant.

The relative permeability of P_{NMDG}/P_{Na} was estimated using the Goldman–Hodgkin–Katz voltage equation:

$$V_{rev} = \frac{RT}{F} \ln\left(\frac{P_{Na}[Na]_{out} + P_{NMDG}[NMDG]_{out}}{P_{Na}[Na]_{in} + P_{NMDG}[NMDG]_{in}}\right).$$

The time constants for MTS reagents modification (τ) were obtained by fitting a single-exponential function to current relaxations using the equation:

$$f(t) = \sum_{i=0}^{n} A_i e^{-t/\tau_i} + C,$$

and modification rates (R) were calculated according to the following:

$$R = \frac{1}{\tau[M]},$$

where [M] is the concentration of the thiol-reactive reagent (MTS-ET or MTS-TPAE).

Immunolabeling and Microscopy. HEK 293 cells were seeded at a ~60% confluency on round glass coverslips (18 mm; Warner Instruments) in DMEM (Gibco), supplemented with 10% FBS (Gibco) and 0.5% gentamicin (Gibco) for 10 to 15 h at 37 °C, and then transfected with 500 to 900 ng DNA per well using the Fugene 6 reagent (Promega). After 18 to 24 h, cells were fixed using 2% paraformaldehyde in PBS for 20 min and permeabilized with 0.2% Triton X-100 in PBS (Gibco). Cells were then incubated overnight at 4 °C with rabbit polyclonal anti-P2X2 receptor primary antibody (APR-003; Alomone) at a 1:1,000 dilution in PBS with 10% Probumin BSA (Millipore). Cells were then washed 3 to 4 times with PBS to remove unbound antibody, and then incubated with secondary Alexa Flour 555-conjugated goat anti-rabbit antibody (Thermo Fisher Scientific) at a 1:1,000 dilution in PBS with 10% Probumin BSA for 20 min at room temperature, followed by 4 to 5 further washes with PBS. To label F-actin, cells were stained with Alexa Fluor 647 Phalloidin (Thermo Fisher Scientific) at a 1:50 dilution in 10% Probumin BSA in PBS for 20 min, and then the excess of Phalloidin was washed 3 times with PBS. Stained cells were mounted for imaging on microscopy slides (Daigger; 1 mm) using mounting media ProLong Diamond Antifade Mountant (Invitrogen) and set to cure for at least 24 h.

Imaging was performed in the Microscopy and Imaging Core (National Institute of Child Health and Development) using a laser-scanning confocal microscope (LSM 780; Carl Zeiss) with a Plan-Apochromat 63× objective (numerical aperture, 1.4). The following laser lines: 488, 561, and 633 nm, were used to excite Clover, Alexa Fluor 555, and Alexa Fluor 647, respectively. A z stack of images was collected from the top to bottom of the cell with 0.36- to 0.45-μm z-step intervals. All images were acquired using Zeiss ZEN Black 2.3 SP1 software (Carl Zeiss) and processed/analyzed using Fiji open-source image-processing package (61).

ACKNOWLEDGMENTS. We thank Angela Ballesteros, Orsolya Szilagyi, and members of the K.J.S. laboratory for helpful discussions and Vincent Schram from the National Institute of Child Health and Development Microscopy and Imaging Core for assisting in the confocal image acquisition. This work was supported by the Intramural Research Programs of the National Institute of Neurological Disorders and Stroke–NIH (to K.J.S.).

1. R. A. North, Molecular physiology of P2X receptors. *Physiol. Rev.* **82**, 1013–1067 (2002).
2. B. S. Khakh, R. A. North, P2X receptors as cell-surface ATP sensors in health and disease. *Nature* **442**, 527–532 (2006).
3. G. D. Housley *et al*., ATP-gated ion channels mediate adaptation to elevated sound levels. *Proc. Natl. Acad. Sci. U.S.A.* **110**, 7494–7499 (2013).
4. G. D. Housley *et al*., Purinergic regulation of sound transduction and auditory neurotransmission. *Audiol. Neurotol.* **7**, 55–61 (2002).
5. A. Saul, R. Hausmann, A. Kless, A. Nicke, Heteromeric assembly of P2X subunits. *Front. Cell. Neurosci.* **7**, 250 (2013).
6. T. Kawate, J. C. Michel, W. T. Birdsong, E. Gouaux, Crystal structure of the ATP-gated $P2X_4$ ion channel in the closed state. *Nature* **460**, 592–598 (2009).
7. T. Sueta, B. Paki, A. W. Everett, D. Robertson, Purinergic receptors in auditory neurotransmission. *Hear. Res.* **183**, 97–108 (2003).
8. Z. Xiang, X. Bo, G. Burnstock, P2X receptor immunoreactivity in the rat cochlea, vestibular ganglion and cochlear nucleus. *Hear. Res.* **128**, 190–196 (1999).
9. G. D. Housley, Physiological effects of extracellular nucleotides in the inner ear. *Clin. Exp. Pharmacol. Physiol.* **27**, 575–580 (2000).
10. N. Yu, H. B. Zhao, ATP activates P2x receptors and requires extracellular Ca^{++} participation to modify outer hair cell nonlinear capacitance. *Pflugers Arch.* **457**, 453–461 (2008).
11. P. R. Thorne, D. J. Muñoz, G. D. Housley, Purinergic modulation of cochlear partition resistance and its effect on the endocochlear potential in the guinea pig. *J. Assoc. Res. Otolaryngol.* **5**, 58–65 (2004).
12. E. Berekméri, J. Szepesy, L. Köles, T. Zelles, Purinergic signaling in the organ of Corti: Potential therapeutic targets of sensorineural hearing losses. *Brain Res. Bull.* **151**, 109–118 (2019).
13. U. Brändle, H. P. Zenner, J. P. Ruppersberg, Gene expression of P2X-receptors in the developing inner ear of the rat. *Neurosci. Lett.* **273**, 105–108 (1999).
14. L. E. Järlebark, G. D. Housley, P. R. Thorne, Immunohistochemical localization of adenosine 5′-triphosphate-gated ion channel $P2X_2$ receptor subunits in adult and developing rat cochlea. *J. Comp. Neurol.* **421**, 289–301 (2000).

15. R. T. Morton-Jones *et al*., Properties of ATP-gated ion channels assembled from P2X2 subunits in mouse cochlear Reissner's membrane epithelial cells. *Purinergic Signal.* **11**, 551–560 (2015).
16. D. Yan *et al*., Mutation of the ATP-gated $P2X_2$ receptor leads to progressive hearing loss and increased susceptibility to noise. *Proc. Natl. Acad. Sci. U.S.A.* **110**, 2228–2233 (2013).
17. L. E. Järlebark, G. D. Housley, N. P. Raybould, S. Vlajkovic, P. R. Thorne, ATP-gated ion channels assembled from P2X2 receptor subunits in the mouse cochlea. *Neuroreport* **13**, 1979–1984 (2002).
18. G. D. Housley *et al*., Expression of the $P2X_2$ receptor subunit of the ATP-gated ion channel in the cochlea: Implications for sound transduction and auditory neurotransmission. *J. Neurosci.* **19**, 8377–8388 (1999).
19. J. C. Wang *et al*., Noise induces up-regulation of P2X2 receptor subunit of ATP-gated ion channels in the rat cochlea. *Neuroreport* **14**, 817–823 (2003).
20. R. S. Telang *et al*., Reduced $P2x_2$ receptor-mediated regulation of endocochlear potential in the ageing mouse cochlea. *Purinergic Signal.* **6**, 263–272 (2010).
21. F. Faletra *et al*., A novel P2RX2 mutation in an Italian family affected by autosomal dominant nonsyndromic hearing loss. *Gene* **534**, 236–239 (2014).
22. H. Moteki *et al*., Hearing loss caused by a P2RX2 mutation identified in a MELAS family with a coexisting mitochondrial 3243AG mutation. *Ann. Otol. Rhinol. Laryngol.* **124** (suppl. 1), 177S–183S (2015).
23. S. H. Blanton *et al*., A novel locus for autosomal dominant non-syndromic deafness (DFNA41) maps to chromosome 12q24-qter. *J. Med. Genet.* **39**, 567–570 (2002).
24. S. E. Mansoor *et al*., X-ray structures define human $P2X_3$ receptor gating cycle and antagonist action. *Nature* **538**, 66–71 (2016).
25. G. Kasuya *et al*., Structural insights into divalent cation modulations of ATP-gated P2X receptor channels. *Cell Rep.* **14**, 932–944 (2016).
26. A. Karasawa, T. Kawate, Structural basis for subtype-specific inhibition of the P2X7 receptor. *eLife* **5**, e22153 (2016).
27. J. Wang *et al*., Druggable negative allosteric site of P2X3 receptors. *Proc. Natl. Acad. Sci. U.S.A.* **115**, 4939–4944 (2018).
28. Y. Zhu, J. Beudez, N. Yu, T. Grutter, H. B. Zhao, P2X2 dominant deafness mutations have no negative effect on wild-type isoform: Implications for functional rescue and in deafness mechanism. *Front. Mol. Neurosci.* **10**, 371 (2017).
29. S. W. Rothwell, P. J. Stansfeld, L. Bragg, A. Verkhratsky, R. A. North, Direct gating of ATP-activated ion channels (P2X2 receptors) by lipophilic attachment at the outer end of the second transmembrane domain. *J. Biol. Chem.* **289**, 618–626 (2014).
30. L. Cao, H. E. Broomhead, M. T. Young, R. A. North, Polar residues in the second transmembrane domain of the rat P2X2 receptor that affect spontaneous gating, unitary conductance, and rectification. *J. Neurosci.* **29**, 14257–14264 (2009).
31. K. J. Lynch *et al*., Molecular and functional characterization of human $P2X_2$ receptors. *Mol. Pharmacol.* **56**, 1171–1181 (1999).
32. Z. Zhou, R. I. Hume, Two mechanisms for inward rectification of current flow through the purinoceptor P2X2 class of ATP-gated channels. *J. Physiol.* **507**, 353–364 (1998).
33. Y. Fujiwara, B. Keceli, K. Nakajo, Y. Kubo, Voltage- and [ATP]-dependent gating of the $P2X_2$ ATP receptor channel. *J. Gen. Physiol.* **133**, 93–109 (2009).
34. M. Li, T. H. Chang, S. D. Silberberg, K. J. Swartz, Gating the pore of P2X receptor channels. *Nat. Neurosci.* **11**, 883–887 (2008).
35. M. Horie, H. Irisawa, A. Noma, Voltage-dependent magnesium block of adenosine-triphosphate-sensitive potassium channel in guinea-pig ventricular cells. *J. Physiol.* **387**, 251–272 (1987).
36. H. Matsuda, A. Saigusa, H. Irisawa, Ohmic conductance through the inwardly rectifying K channel and blocking by internal Mg^{2+}. *Nature* **325**, 156–159 (1987).
37. C. A. Vandenberg, Inward rectification of a potassium channel in cardiac ventricular cells depends on internal magnesium ions. *Proc. Natl. Acad. Sci. U.S.A.* **84**, 2560–2564 (1987).
38. Z. Lu, R. MacKinnon, Electrostatic tuning of Mg^{2+} affinity in an inward-rectifier K^+ channel. *Nature* **371**, 243–246 (1994).
39. A. N. Lopatin, C. G. Nichols, Internal Na^+ and Mg^{2+} blockade of DRK1 (Kv2.1) potassium channels expressed in Xenopus oocytes. Inward rectification of a delayed rectifier. *J. Gen. Physiol.* **103**, 203–216 (1994).
40. M. Li, G. E. Toombes, S. D. Silberberg, K. J. Swartz, Physical basis of apparent pore dilation of ATP-activated P2X receptor channels. *Nat. Neurosci.* **18**, 1577–1583 (2015).
41. M. Harkat *et al*., On the permeation of large organic cations through the pore of ATP-gated P2X receptors. *Proc. Natl. Acad. Sci. U.S.A.* **114**, E3786–E3795 (2017).
42. C. Virginio, R. A. North, A. Surprenant, Calcium permeability and block at homomeric and heteromeric P2X2 and P2X3 receptors, and P2X receptors in rat nodose neurones. *J. Physiol.* **510**, 27–35 (1998).
43. R. J. Evans *et al*., Ionic permeability of, and divalent cation effects on, two ATP-gated cation channels (P2X receptors) expressed in mammalian cells. *J. Physiol.* **497**, 413–422 (1996).
44. M. Li, T. Kawate, S. D. Silberberg, K. J. Swartz, Pore-opening mechanism in trimeric P2X receptor channels. *Nat. Commun.* **1**, 44 (2010).
45. C. Coddou, Z. Yan, T. Obsil, J. P. Huidobro-Toro, S. S. Stojilkovic, Activation and regulation of purinergic P2X receptor channels. *Pharmacol. Rev.* **63**, 641–683 (2011).
46. C. A. Trujillo *et al*., Inhibition mechanism of the recombinant rat $P2X_2$ receptor in glial cells by suramin and TNP-ATP. *Biochemistry* **45**, 224–233 (2006).
47. P. Leff, B. E. Wood, S. E. O'Connor, Suramin is a slowly-equilibrating but competitive antagonist at P2x-receptors in the rabbit isolated ear artery. *Br. J. Pharmacol.* **101**, 645–649 (1990).
48. S. Valera *et al*., A new class of ligand-gated ion channel defined by P2x receptor for extracellular ATP. *Nature* **371**, 516–519 (1994).
49. R. J. Evans *et al*., Pharmacological characterization of heterologously expressed ATP-gated cation channels (P2x purinoceptors). *Mol. Pharmacol.* **48**, 178–183 (1995).
50. L. Cao, M. T. Young, H. E. Broomhead, S. J. Fountain, R. A. North, Thr339-to-serine substitution in rat P2X2 receptor second transmembrane domain causes constitutive opening and indicates a gating role for Lys308. *J. Neurosci.* **27**, 12916–12923 (2007).
51. F. Soto, G. Lambrecht, P. Nickel, W. Stühmer, A. E. Busch, Antagonistic properties of the suramin analogue NF023 at heterologously expressed P2X receptors. *Neuropharmacology* **38**, 141–149 (1999).
52. R. A. North, A. Surprenant, Pharmacology of cloned P2X receptors. *Annu. Rev. Pharmacol. Toxicol.* **40**, 563–580 (2000).
53. J. A. Sim, H. E. Broomhead, R. A. North, Ectodomain lysines and suramin block of P2X1 receptors. *J. Biol. Chem.* **283**, 29841–29846 (2008).
54. M. Garcia-Guzman, F. Soto, J. M. Gomez-Hernandez, P. E. Lund, W. Stühmer, Characterization of recombinant human P2X4 receptor reveals pharmacological differences to the rat homologue. *Mol. Pharmacol.* **51**, 109–118 (1997).
55. J. Molnár, G. Szakács, G. E. Tusnády, Characterization of disease-associated mutations in human transmembrane proteins. *PLoS One* **11**, e0151760 (2016).
56. F. Rassendren, G. Buell, A. Newbolt, R. A. North, A. Surprenant, Identification of amino acid residues contributing to the pore of a P2X receptor. *EMBO J.* **16**, 3446–3454 (1997).
57. P. Wangemann, Supporting sensory transduction: Cochlear fluid homeostasis and the endocochlear potential. *J. Physiol.* **576**, 11–21 (2006).
58. R. Fettiplace, Hair cell transduction, tuning, and synaptic transmission in the mammalian cochlea. *Compr. Physiol.* **7**, 1197–1227 (2017).
59. M. Hattori, E. Gouaux, Molecular mechanism of ATP binding and ion channel activation in P2X receptors. *Nature* **485**, 207–212 (2012).
60. L. H. Jiang, F. Rassendren, V. Spelta, A. Surprenant, R. A. North, Amino acid residues involved in gating identified in the first membrane-spanning domain of the rat $P2X_2$ receptor. *J. Biol. Chem.* **276**, 14902–14908 (2001).
61. J. Schindelin *et al*., Fiji: An open-source platform for biological-image analysis. *Nat. Methods* **9**, 676–682 (2012).